Mohammed Traiche[1,3], Habib Rached[2], Rami K. Suleiman[4], Mouna Amara[1], Mohammed Hadj Meliani[1*]

PHOTODETECTORS PERFORMANCE OF NANOSTRUCTURED MATERIALS IN ANTIMONY III-V InGaAsSb/AlGaAsSb INTERBAND CASCADE STRUCTURES

PERFORMANSE FOTODETEKTORA OD NANOSTRUKTURIRANIH MATERIJALA U ANTIMON III-V InGaAsSb/AlGaAsSb MEĐUZONSKIM KASKADNIM STRUKTURAMA

Adresa autora / Author's address:
[1] Laboratory of Theoretical Physics and Material Physics, Hassiba Benbouali University of Chlef, Hay Salem, Chlef, Algeria
M. Traiche 0000-0001-6926-0685; M. Hadj Meliani 0000-0003-1375-762X

[2] Faculty of Exact Sciences and Informatics, Hassiba Benbouali University of Chlef, Chlef, Algeria 0000-0003-3867-576X
[3] Faculty of Science and Technology, Hassiba Benbouali University of Chlef, Chlef, Algeria
[4] Interdisciplinary Research Center for Advanced Materials, King Fahd University of Petroleum & Minerals, Dhahran, Saudi Arabia
0000-0002-6776-9266
*email: m.hadjmeliani@univ-chlef.dz

Abstract

The aim of the study is to increase the performance of solar conversion by integrating nanostructured materials within conventional solar cells by employing multi-energy stages (i.e., interband and intersubband) in cascade systems to overcome the absorption length barrier and achieve large photo-generated carrier values. Specifically, InGaAsSb/Al GaAsSb MQWs are investigated with narrow well widths (2-20 nm) and transition energies of the structures are calculated for varied well/barrier widths and depths using numerical modelling. The results show that both interband and intersubband transitions are valuable for improving photovoltaic and photodetection applications, but their mechanisms and applications are distinct, so understanding and controlling these transitions within semiconductor materials is essential for optimising the performance of devices in both areas of optoelectronics, including strain as an important parameter of integrity. The data suggests that a single electron requires multiple photons to be transported, with the formation of a type-I broken-gap alignment between AlGa AsSb (barrier) and InGaAsSb (well). A wide range of wavelengths, from visible to medium infrared (MIR), will greatly enhance solar spectrum absorption. The long-term goal is to combine the thermal properties of antimonies (GaSbInSb) with a low band gap and the optical properties of arsenide (GaAsAlAs) with a large band gap.

Izvod

Cilj studije je povećanje performanse solarne konverzije, integracijom nanostrukturiranih materijala unutar konvencionalnih solarnih ćelija upotrebom višeenergetskih nivoa (na pr. unutar-zonski i unutar-podzonski) u kaskadnim sistemima, kako bi se prevazišla barijera dužine apsorpcije i postigle velike fotogenerisane vrednosti nosioca. Konkretno, višestruki kvantni ponori InGaAsSb/AlGaAsSb su istraženi sa uskim širinama ponora (2-20 nm), a prelazne energije nivoa struktura su izračunate numeričkim modeliranjem za različite širine i dubine ponora/barijera. Rezultati pokazuju da su unutarpojasni i unutarpodpojasni prelazi značajni za poboljšanje fotonaponskih i fotodetekcionih aplikacija, ali su njihovi mehanizmi i primene različiti, tako da je razumevanje i upravljanje ovim prelazima u poluprovodničkim materijala od suštinskog značaja za optimizaciju performansi uređaja u oba područja optoelektronike, uključujući i deformaciju kao važan parametar integriteta. Podaci sugerišu da je za transport jednog elektrona potrebno više fotona, uz formiranje zabranjene zone tipa I između AlGaAsSb (barijere) i InGaAsSb (ponora). Širok raspon talasnih dužina, od vidljivih do srednje infracrvenih (MIR), uvelike će poboljšati apsorpciju sunčevog spektra. Dugoročni cilj je da se kombinuju termička svojstva antimona (GaSbInSb) sa malom zabranjenom zonom i optička svojstva arsenida (GaAsAlAs) sa velikom zabranjenom zonom.

INTRODUCTION

Nanostructured materials have played a significant part in the manufacture of thermoelectric devices, /1/. Introducing quantum wells (QW) in the middle subcell is found to be one of the promising approaches, Here, the intrinsic region of p-n junction is replaced with p-i-n, where the quantum wells (QW) and quantum barriers (QB) are inserted in the intrinsic area, many studies have shown higher radiation resistance by using QW and QB within the intrinsic region for many

III-V materials families, /2/. The strong and uniform electric field in the intrinsic region led to a good effective carrier's transport across the device, /3/. A theoretical model of PIN junction containing quantum wells, /4/, formed by a quaternary system $In_xGa_{1-x}As_ySb_{1-y}$ for wells and $Al_xGa_{1-x}As_ySb_{1-y}$ for barriers was described by K. Mamic, A. Bainbridge, et al /5/. Three potential strategies have been investigated in order to increase MQW solar cells' efficiency even more. The first approach is avoiding thermal losses by using thermoelectric materials with direct band gap, /6/; the second

approach is the possibility to effectively convert a great part of solar spectrum by shifting the energy levels in the QWs through the modification of the geometry of QW and BW /7/; the third approach is to improve overall photon absorption. Thus, the ideal case consists of two sub-bands that are parallel QW type-I, Fig. 1a, where the density of states reaching a single symmetric peak, Fig. 1b, leads to strong resonant absorption when the incident photon energy coincides with the sub-band separation.
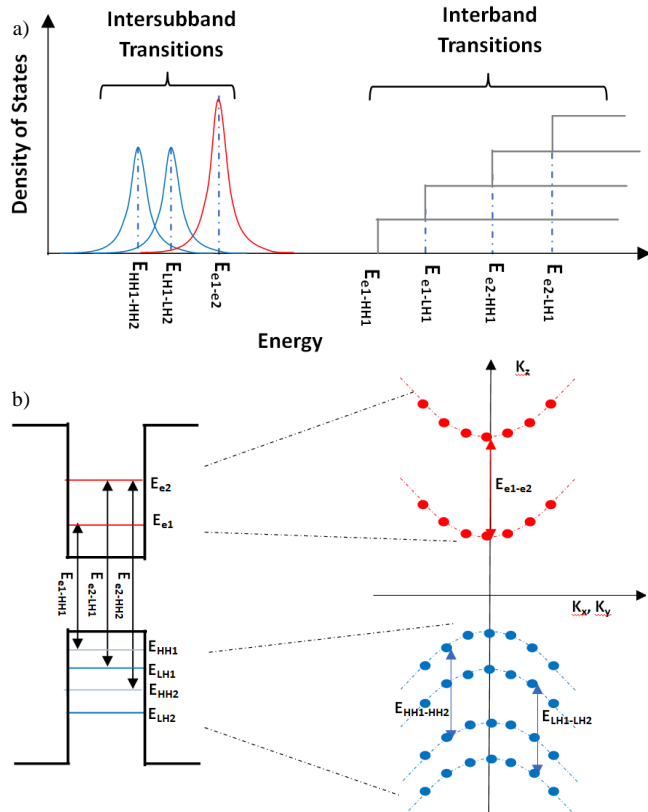

Figure 1. Schematic diagram for finite quantum well type-I
a) illustrations of permitted intersubband and interband transitions;
b) the density of states for intersubband and interband transitions.

The most important characteristics of such structures are found to be the width, depth and number of quantum wells, /8/. Introducing quantum wells in the middle subcell is found to be one of the promising approaches, /4/. There is a need to increase the performance of solar conversion by integrating nanostructured materials within conventional solar cells by employing multi-energy stages (i.e., interband and inter-subband), /9/, in cascade systems to overcome the absorption length barrier and achieve large photo-generated carrier values.

Intersubband transitions are crucial for efficient detection and conversion of specific wavelengths in photodetectors, especially in the infrared spectrum, /10/. Specifically, InGaAsSb/AlGaAsSb MQWs are investigated with narrow well widths (2-20 nm) and transition energies of the structures are calculated for varied well/barrier widths and depths using numerical modelling.

METHODOLOGY

Device design engineering and structural optimisation

The III-V family based on antimonide alloys are employed since these materials offer optimal narrow bandgap energy while keeping the lattice-matched condition and, therefore, enabling designs shown in Fig. 2.
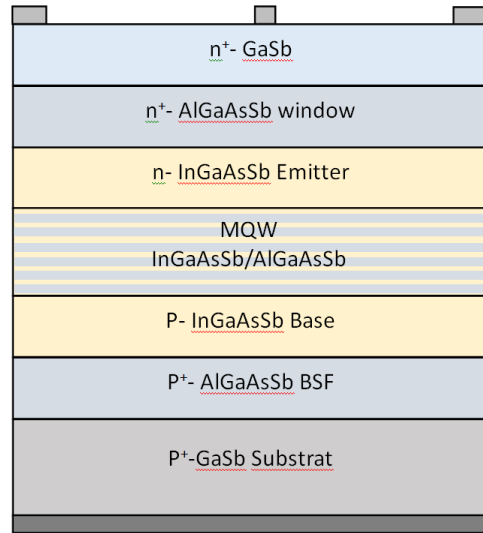

Figure 2. Structure of a PIN thermophotovoltaic solar cell with multi quantum wells.

Approach based on the band diagram and strain engineering to obtain type I quantum wells based InGaAsSb/AlGaAsSb /11/ for infrared detector on GaSb substrate, takes into consideration a quantum well type I, lattice-mismatch within 2 % (circles in Fig. 3), and good band offset to gain good confinement for both - electrons and holes (Table 1). Study on the optimisation of materials was done using a quaternary alloy formed by the two families of III-V semiconductors, arsenide and antimonide. The structure shown in Fig. 2 is made on a GaSb substrate followed by an N-type GaSb layer and then a buffer layer of AlGaAsSb to ensure mesh agreement with the active zone which will constitute multi-quantum wells AlGaAsSb/InGaAsSb, then a second buffer layer was made by AlGaAsSb with a concentration
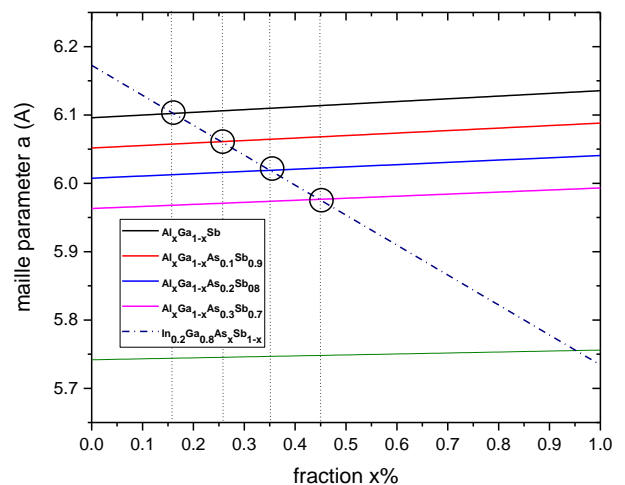

Figure 3. Calculation of $Al_xGa_{1-x}As_ySb_{1-y}/In_{0.2}Ga_{0.8}As_xSb_{1-x}$ mesh parameter as a function of composition.

Table 1. The scheme of the layer's composition in investigated samples.

Sample	A	B	C	D
QW	$In_{0.2}Ga_{0.8}As_{0.15}Sb_{0.85}$	$In_{0.2}Ga_{0.8}As_{0.25}Sb_{0.75}$	$In_{0.2}Ga_{0.8}As_{0.35}Sb_{0.65}$	$In_{0.2}Ga_{0.8}As_{0.45}Sb_{0.55}$
Barrier	$Al_{0.15}Ga_{0.85}Sb$	$Al_{0.26}Ga_{0.74}As_{0.1}Sb_{0.9}$	$Al_{0.35}Ga_{0.65}As_{0.2}Sb_{0.8}$	$Al_{0.45}Ga_{0.55}As_{0.3}Sb_{0.7}$
ΔE_C (eV)	0.21	0.34	0.42	0.62
ΔE_V (eV)	0.06	0.17	0.30	0.24

different from that on the first terminal, to ensure the mesh agreement between the active zone and the second pole of the junction which is a typical GaAs layer P-type.

The first part of our work seeks to find the best adjustment of the energy gap according to the lattice mismatch. The composition dependence of the lattice parameter is described by the linear variation law, /12/, given by Eq.(1):

$$a_{ABCD}(x,y) = x[ya_{AC} + (1-y)a_{AD}] + y(1-x)a_{BC} + (1-x)(1-y)a_{BD}. \quad (1)$$

The dashed line in Fig. 3 shows the variation of the lattice parameter of InGaAsSb as a function of As concentration by taking a low fraction of indium 20 % in the wells to obtain a narrow band gap, and demonstrates how the lattice parameter of AlGaAsSb can vary depending on the lattice parameter for Al composition in the barrier and As composition in the well with a significant amount of GaSb up to 50 % to gain good thermal proprieties of antimony alloys /5/ and reduce compressive strain, /13/. Figure 3 shows a good mesh agreement for different values, indicating that several options are available as designated by circles. Maintaining good mesh agreement is an iterative process, requiring multiple iterations of mesh refinement and analysis to achieve accurate results, as overly refined good mesh with desired proprieties can lead to longer simulation times.

The energy bandgap is calculated by Eq.(2), based on the work of Vurgaftman et al. /12/,

$$E_{(ABCD)}(x,y) = x(1-x)\frac{[yE_{(ABC)} + (1-y)E_{(ABD)}]}{x(1-x) + y(1-y)} + y(1-y)\frac{[xE_{(ACD)} + (1-x)E_{(BDC)}]}{x(1-x) + y(1-y)}. \quad (2)$$

Bandgap energies of InGaAsSb quaternary system extend from 0.17 eV for InSb to 1.42 eV for GaAs and the energy gap of AlGaAsSb ranges between 0.72 for GaSb and 2.30 for AlSb, /14/, Fig. 4.
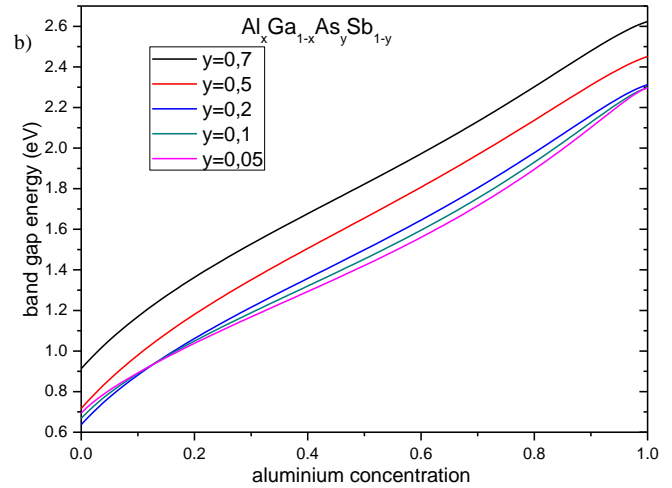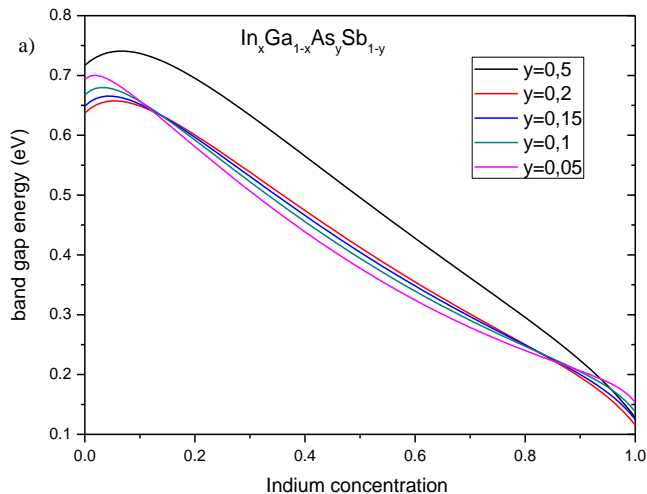
Figure 4. a) Variations of gap energy as a function of x (% In) and for different y (% As); b) variations of gap energy as a function of x (% Al) and for different y (% As).

Variations shown in Figs. 4a and 4b of E_G is a nonlinear variation, for $In_xGa_{1-x}As_ySb_{1-y}$ the energy gap decreases sturdily with indium fraction so to reach narrow bandgap range 0.5 eV < E_G < 0.7 eV and keep the lattice mismatch within the acceptable limit $\Delta a/a$ < 2 %.

Findings derived by Eq.(2) correspond well with experimental data for energy gaps E_G for Γ, X and L valleys, as well as the spin-orbit splitting of many III-V quaternary systems. The E_G obtained from Eq.(2) are plotted in Fig. 4 as a function of x with different value of y for: a) $In_xGa_{1-x}As_ySb_{1-y}$, and b) $Al_xGa_{1-x}As_ySb_{1-y}$, respectively.

RESULTS AND DISCUSSION

As it is intended to incorporate a large antimony composition, above 0.5, so it is necessary to limit x < 25 % of indium and y < 30 % of arsenic, /15/. For barrier AlGaAsSb, E_G depends mainly on Al fraction, but the lattice parameter depends much on x in Al, as shown in Fig. 2, and especially on y in As. So, to realise QWs based on InGaAsSb on the barrier based on system AlGaAsSb we must impose values of y < 30 %. Moreover, the barrier conduction band and valence band are shifted due to the high arsenic fraction in the barrier up to 10 % and high indium fraction 20 % in the QWs to ensure a better confinement /15, 16/, as shown in Table 1, and thus generate a compressive strain requiring precise strain balancing. For this reason, we propose different superlattice designs for QWs and barrier, then report the demonstration of high-performance photodetectors based on InGaAsSb/AlGaAsSb type-I superlattices, and we apply the theoretical model to calculate the band offset. The proposed material's systems in the Table 1 enable the construction of multiple QWs integrated in PIN junction with even several possibilities to create type I QWs, /14/, which may further increase the conversion efficiency. This highly required fea-

ture is available with this material's system that can be a grown lattice matched on GaSb and/or GaAs substrates, /16/.

To reach high performance PIN photodetectors, two principal challenges need to be overcome. The first one resides in choosing an InGaAsSb/AlGaAsSb system with a NIR cut-off wavelength theoretically giving a high absorption coefficient. At the same time, the superlattice design must give a good strain balance to ensure a high-quality material for a long minority carrier diffusion length to achieve high quantum efficiency (QE), /17/. In order to obtain high quantum efficiency, the superlattice design must provide appropriate strain control to guarantee a high-quality material with a long minority carrier diffusion length, /18/. The second challenge is in designing a highly controllable barrier that effectively blocks the majority of electrons in the conduction band while ensuring free movement of minority holes in the valence band.

INTERSUBBAND AND INTERBAND OPTICAL TRANSITIONS IN QUANTUM WELL

The calculation procedures described here follow the envelope function approach based on effective-mass approximation, /13/, to obtain in-plane subband dispersions in the conduction and valence band. The Schrodinger equation for a particle of mass m confined in 1D potential well in an electric field E perpendicular to the quantum well layer is given by Eq.(3), /14/:

$$i\hbar \frac{\partial \psi}{\partial t}(x,t) = \left(-\frac{h^2}{2m}\frac{\partial^2}{\partial x^2} + V(x) \right)\psi(x,t) . \quad (3)$$

The set of energies E_n and stationary states φ_n, form the eigenvalues and eigenstates of the Hamiltonian operator

$$\hat{H}\varphi_n = \left(-\frac{h^2}{2m}\frac{\partial^2}{\partial x^2} + V(x) \right)\varphi_n = E_n\varphi_n . \quad (4)$$

We use the effective mass approximation to calculate the energy states for a quantum well, /12/,

$$\left(-\frac{h^2}{2m^*}\frac{\partial^2}{\partial x^2} + V(x) \right)\varphi_n = E_n\varphi_n , \quad (5)$$

$$\varphi''(x) = \frac{2m^*(V_0 - E)}{h^2}\varphi , \quad (6)$$

$$\varphi''(x) = -k^2\varphi , \quad (7)$$

$$\begin{cases} k = \sqrt{\dfrac{2m_{e,h}^* E}{h^2}} & -\dfrac{L}{2} \leq x \leq \dfrac{L}{2} \\[4mm] k = \sqrt{\dfrac{2m_{e,h}^*(E - V_0)}{h^2}} & x > \dfrac{L}{2} \text{ or } x < -\dfrac{L}{2} \end{cases} . \quad (8)$$

The relation between number of energy state and the energy of confinement is given by the relations:

$$\sqrt{2m_{e,h}^* E_n}\left(\frac{L}{h} \right) = n\pi , \quad (9)$$

$$E_n \leq \Delta E_{C,V} . \quad (10)$$

We obtain:

$$E_n = \frac{n^2\pi^2}{2m_{e,h}^*}\frac{h^2}{L^2} , \quad (11)$$

where: $n = 1, 2, …$ energy levels; $m_{e,h}^*$ is effective mass of electrons or holes, respectively; L is width of the well; $\hbar = h/2\pi$.

$$\phi_n = A\sin\left(\frac{n\pi z}{L_z} \right) . \quad (12)$$

So, the number of energy states n is given by:

$$\sqrt{2m_{e,h}^* \Delta E_{C,V}}\left(\frac{L}{h} \right) > n . \quad (13)$$

The number of discrete energy levels n strongly depends on the value of the offset band $\Delta E_{C,V}$, the effective mass of the carriers $m_{e,h}^*$ and the width of the well L.

All possible direct transitions are calculated as a function of QW width to recognise how to design devices for different wavelength section.

Intersubband transition in CB

The selection rule instead of momentum conservation, asserts that only transitions between states of the same quantum number in valence and conduction bands are allowed (Figs. 5 and 6), /19/. Intersubband spacing between the energy levels for electrons, Fig. 5, and holes, Fig. 6, are different due to their different effective mass, /22/. Figure 5 presents the main intersubband optical transitions in CB as a function of quantum well width. As can be observed modelling starts at 2 nm QW width steps between 2 and 20 nm, and the resulting transitions are plotted with the barrier width fixed at 0.62 eV to maintain strain symmetrisation throughout all the modelled structures.

As shown in Fig. 5 for QW width between 5 and 20 nm the splitting between E_1 and E_2 increase inversely proportional, /20/, but when QW width is less than 5 nm the splitting decreases due to the correlation between the 2nd energy state and the 1st and 3rd energy states.

Other transitions are possible as mentioned in Eqs.(9-10), where the number of energy states that can appear depends on ΔE_C. For example, for three levels of energy, another two transitions between $e_1 - e_3$ and $e_2 - e_3$, the splitting between those levels decreases when QW width increases, until they merge when the material is in the bulk state.
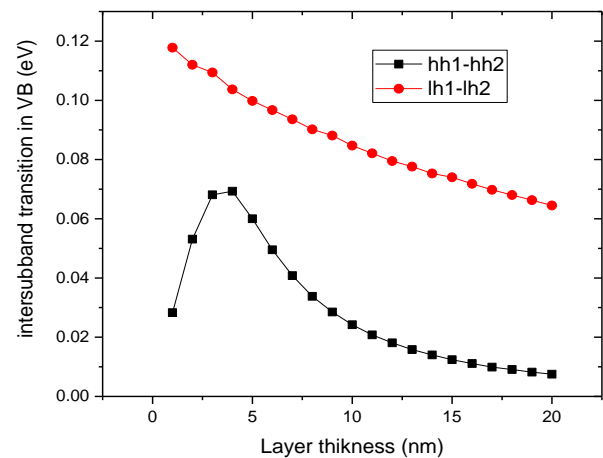
Figure 5. Intersubband transitions in conduction-confined energies for electrons as a function of barrier thickness, at 300 K.

Light and heavy holes intersubband transition

In general, there are two types of holes with different effective masses in semiconductors. They are known as light and heavy holes. Due to the masses of these two types of holes that differ; there exist two sets of holes subbands with different energy spacing. The light holes have a considerably smaller effective mass usually comparable to that of the electron and have its subband spaced further away, compared to heavy holes.

The heavy-hole-to-conduction state has a slightly lower energy and is more closely spaced than the light-hole-to-conduction state, as shown in Fig. 6. The heavy hole state is usually dominant in optical absorption for light propagation perpendicular to the quantum well layers /19, 21/. For intersubband transitions, heavy hole HH_1 to HH_2 and light hole LH_1 to LH_2 produce only z-polarised absorption in the parabolic band approximation, /21/. HH to LH transitions produced in 3 directions x, y, and z-polarisation but due to the non-parabolicity of the effective masses of holes, the xy-polarization will be reduced significantly because of the confinement in directions xy and the mixing of sub-band, /21/.
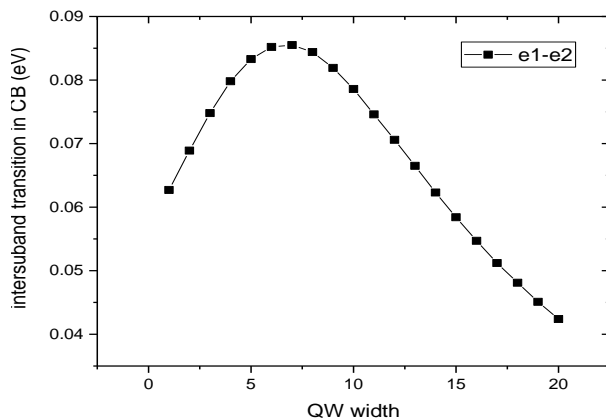

Figure 6. Intersubband transitions in valence-confined energies for heavy and light holes as function of barrier thicknesses at 300 K.

Interband transitions in quantum well

During interband transitions electrons migrate from energy levels in the valence band to another energy level in the conduction band. Interband transitions entail electrons moving from an energy level in the VB to another in the CB, Fig. 7. The energy difference between the initial and final states represents the energy received or released by the photon throughout the transition, /22/. As function of width and material qualities, quantum wells dictate their energy levels, adjusting that these factors can result a controllable interband transition. This tunability is very useful in creating optoelectronic devices with specified absorption wavelengths, such as quantum well photodetectors with high rate of photo-absorption, /22/.

As described previously many discrete energies states for both electrons and holes are possible. We may presume that by applying the energies of the valence confined state for holes and the conduction confined state for electrons, we can obtain different transition energies of the QW structure, calculated as shown in Fig. 7. For widths around 20

nm, the conduction confined states for electrons are therefore nominal around 0.045 eV. However, the valence-confined energies states for light holes are about 0.07 eV, but for heavy holes it is negligible, Figs. 5 and 6. The difference between the two cases is 0.025 eV. On the other hand by decreasing QW width, the difference decreases for QW width up to 5 nm, for widths less than 5 nm the electrons undergo stress caused by the deformation of the mesh of the structure which causes a correlation of the sub-band. This stress effects heavy holes too which express the variation in the form of a saw-tooth graph (Fig. 7) for the transitions e_1-LH_1 and e_2-LH_2. The saw-tooth graph due to confinement effects and anisotropy of the band structure can be further enhanced or modified due to confinement effects. The confinement of carriers in one or more dimensions leads to the quantization of energy levels. The confinement can also modify the band structure and effective mass of holes. The hole mass can become different along the confined direction compared to unconfined directions. In Fig. 7 we observe orientation change along one direction that leads to orientation-dependent electronic and optical properties. Understanding and controlling the directional dependence of the hole mass in nanostructures is crucial for designing and optimising nanoscale devices, such as quantum well photodetector or quantum dot solar cells, and spintronic devices. By engineering the hole mass along specific directions, it is possible to tailor the electronic and optical properties of the nanostructure for specific applications.
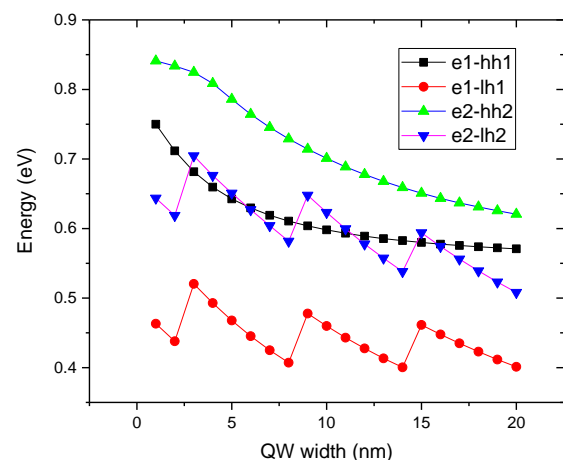

Figure 7. Interband transitions between different confined subband states of CB and VB as a function of QW width at 300 K.

CONCLUSIONS

Simulation results show that by engineering the properties of InGaAsSb-based quantum well photodetectors, such as its depth and width, and by tuning the composition of the InGaAsSb material, it is possible to control the energy levels within the well, to make it sensitive to cover a broad band of wavelengths from visible to mid-infrared. Understanding and controlling the directional dependence of the hole mass in nanostructures is crucial for designing and optimising nanoscale devices, such as quantum well photodetector or emitter, quantum dot solar cells, and spintronic devices. By engineering the hole mass along specific directions, it is possible to tailor the electronic and optical properties of the

nanostructure for specific applications. In the long term this work will help to increase the performance of solar conversion, by integrating nanostructured materials within conventional solar cells using interband and intersubband energy levels in solar cells aimed to increase light absorption, adjust the bandgap to the solar spectrum, decrease energy losses, and improve charge carrier production and collection. These methods have the potential to dramatically improve the efficiency and performance of solar cells, keeping in mind at the same time their integrity which is at sufficient level as long as strains are controlled and maintained at a low level.

REFERENCES

1. Shtern, M., Sherchenkov, A., Shtern, Y., et al. (2023), *Mechanical properties and thermal stability of nanostructured thermoelectric materials on the basis of PbTe and GeTe*, J Alloys Compounds, 946: 169364. doi: 10.1016/j.jallcom.2023.169364

2. Kotamraju, S., Sukeerthi, M., Puthanveettil, S.E. (2019), *Modeling of InGaP/InGaAs-GaAsP/Ge multiple quantum well solar cell to improve efficiency for space applications*, Solar Energy, 186: 328-334. doi: 10.1016/j.solener.2019.05.015

3. Sukeerthi, M., Kotamraju, S. (2021), *Trap and carrier removal study of 4J InGaP/InGaAs-GaAsP MQW/InGaAsNSb/Ge high efficient space solar cell using advanced physical models*, J Phys. E: Low-dimens. Syst. Nanostr. 134: 114914. doi: 10.1016/j.physe.2021.114914

4. Cabrera, C.I., Rimada, J.C., Connolly, J.P., Hernandez, L. (2013), *Modelling of GaAsP/InGaAs/GaAs strain-balanced multiple-quantum well solar cells*, J Appl. Phys. 113(2): 024512. doi: 10.1063/1.4775404

5. Mamic, K., Bainbridge, A., Hanks, L.A., et al. (2023), *InGaAsSb for cut-off tuned SWIR detectors*, In: Proc. Vol. 12430 Quantum Sensing and Nano Electronics and Photonics XIX, SPIE OPTO, San Francisco, CA, 2023. doi: 10.1117/12.2650772

6. Pornrungroj, C., Andrei, V., Reisner, E. (2023), *Thermoelectric-photoelectrochemical water splitting under concentrated solar irradiation*, J Amer. Chem. Soc. 145(25): 13709-13714. doi: 10.1021/jacs.3c01892

7. Ghosh, S., Sarkar, D., Bastia, S., Chaudhary, Y.S. (2023), *Band-structure tunability via the modulation of excitons in semiconductor nanostructures: manifestation in photocatalytic fuel generation*, Nanoscale 15: 10939-10974. doi: 10.1039/D3NR02116E

8. Courel, M., Rimada, J.C., Hernández, L. (2012), *GaAs/GaInNAs quantum well and superlattice solar cell*, Appl. Phys. Lett. 100 (7): 73508. doi: 10.1063/1.3687195

9. Hubbard, S.M., Cress, C.D., Bailey, C.G., et al. (2008), *Effect of strain compensation on quantum dot enhanced GaAs solar cells*, Appl. Phys. Lett. 92(12): 123512. doi: 10.1063/1.2903699

10. Chen, J., Chen, F., Wu, Y., et al. (2023), *Broadband response and a transformation between dual- and single-wavelength detection in coupled doped-well quantum cascade detector*, J Adv. Electr. Mater. 9(7): 2300084. doi: 10.1002/aelm.202300084

11. Héroux, J.B., Pei, C.W., Wang, W.I. (2004), *Epitaxial growth of InGaAsSb/AlGaAsSb heterostructures for mid-infrared lasers based on strain engineering*, J Vacuum Sci. Technol. B, 22(4): 2240-2243. doi: 10.1116/1.1775196

12. Vurgaftman, I., Meyer, J.R., Ram-Mohan, L.R. (2001), *Band parameters for III-V compound semiconductors and their alloys*, J Appl. Phys. 89(11): 5815-5875. doi: 10.1063/1.1368156

13. Haddadi, A., Chen, G., Chevallier, R., et al. (2014), *InAs/InAs$_{1-x}$Sb$_x$ type-II superlattices for high performance long wavelength infrared detection*, Appl. Phys. Lett. 105(12): 121104. doi: 10.1063/1.4896271

14. Adachi, S., Properties of Semiconductor Alloys: Group-IV, III-V and II-VI Semiconductors, John Wiley & Sons, Ltd. ISBN: 978-0-470-74369-0, 2009.

15. Li, W., Héroux, J.B., Wang, W.I. (2004), *Strain-compensated InGaAsSb/AlGaAsSb mid-infrared quantum-well lasers*, Appl. Phys. Lett. 84(12): 2016-2018. doi: 10.1063/1.1687981

16. Kurka, M., Dyksik, M., Suomalainen, S., et al. (2019), *GaInAsSb/AlGa(In)AsSb type I quantum wells emitting in 3 μm range for application in super luminescent diodes*, Opt. Mater. 91: 274-278. doi: 10.1016/j.optmat.2019.03.036

17. Li, J., Saroj, R.K., Slivken, S., et al. (2022), *High performance planar antimony-based superlattice photodetectors using zinc diffusion grown by MBE*, Photonics, 9(9): 664. doi: 10.3390/photonics9090664

18. Razeghi, M. (2020), *9 - InAs/GaSb type II superlattices: A developing material system for third generation of IR imaging*, Mid-infrared Optoelectr. 2020: 379-413. doi: 10.1016/B978-0-08-102709-7.00009-7

19. Jia, C.. Deng, G., Liu, L., et al. (2023), *Antimonide-based high operating temperature infrared photodetectors and focal plane arrays: a review and outlook*, J Phys. D: Appl. Phys. 56(43): 433001. doi: 10.1088/1361-6463/acdefa

20. Yahyaoui, N., Baser, P., Said, M., Saadaoui, S. (2023), *Electric field effect on the intersubband optical absorption of GeSn quantum wells with parabolically graded barriers*, Micro Nanostruct. 184: 207682. doi: 10.1016/j.micrna.2023.207682

21. Huang, W., Li, L., Lei, L., et al. (2018), *Minority carrier lifetime in mid-wavelength interband cascade infrared photodetectors*, Appl. Phys. Lett. 112(25): 251107. doi: 10.1063/1.5030544

22. Ardebili, S.B.S., Kim, J.S., Ha, J., et al. (2023), *Band-to-band transitions in InAs/GaSb multi-quantum-well structures using k.p theory: Effects of well/barrier width and temperature*, Energies, 16(3): 1162. doi: 10.3390/en16031162